

Distance Dependent Localization Approach in Oil Reservoir History Matching: A Comparative Study

*Biniaz Delijani, Ebrahim; Pishvaie, Mahmoud Reza**; Bozorgmehry, Ramin*

*Department of Chemical and Petroleum Engineering, Sharif University of Technology,
P.O. Box 11365-9465 Tehran, I.R. IRAN*

ABSTRACT: *To perform any economic management of a petroleum reservoir in real time, a predictable and/or updateable model of reservoir along with uncertainty estimation ability is required. One relatively recent method is a sequential Monte Carlo implementation of the Kalman filter: the Ensemble Kalman Filter (EnKF). The EnKF not only estimate uncertain parameters but also provide a recursive estimate of system states such as pressures and saturations. Due to high computational cost, however, the EnKF is limited to small size ensemble set in practice. On the other hand small ensemble size yield spurious correlation within covariance of state. A remediation to this problem is to employ covariance localization to remove long-range spurious correlations. In this study, five distance base localization functions have been implemented and analysis on two different cases to obtain a better history matching with EnKF. The results indicate that quartic correlation function produce better results than others especially to the popular fifth-order correlation function meanwhile maintain more total variance at the end of the assimilation.*

KEY WORDS: *History matching, Ensemble Kalman filter, Covariance localization, Correlation functions.*

INTRODUCTION

To establish any optimal plan for petroleum reservoir development in its early stages, a stochastic reservoir model with predictable ability is required. The process to obtain such a predictable model is automated history matching or data assimilation. Traditional history matching techniques utilize production observation in a batch-integrated process to adjust the reservoir model parameters while Data Assimilation (DA) employs the same data sequentially. In addition to this, DA estimates the dynamic data or states of reservoir. During history

matching process, reservoir dynamic data (such as production and 4D seismic) are integrated within geological model to characterize the unknown real reservoir. These unknowns may include both static parameters (permeability and porosity map, initial values and boundaries loci to name few) and system states such as pressures, saturations. Assimilation techniques minimize an objective function that is a combination of data mismatch (discrepancies between the model estimates and the observed/measured data) and model

* To whom correspondence should be addressed.

+ E-mail: pishvaie@sharif.edu

1021-9986/14/1/75

17/\$/3.70

mismatch (difference between the updated/analyzed model parameters and the prior), sequentially. In this method, at any assimilation cycle, model parameters are updated by the use of new observations.

DA, in a Bayesian framework, is an approach to sample posteriori Probability Density Function (PDF) of model parameters through employing production data. A relatively recent method which belongs to this statistical-viewed family and initially was utilized for near well monitoring is Ensemble Kalman Filter (EnKF) [1, 2]. *Gu & Oliver* were first that applied the EnKF for history matching process [3]. Due to advantages of EnKF, it soon became a major research topic in automatic history matching [4]. This method can be readily implemented to any reservoir simulator without requirement for sensitivity calculation. In EnKF, just the cross-covariance of predicted data with model parameters (as a measure of estimation errors) and covariance of predicted data itself (as measure of model improvements offered by measurement) are employed to carry out the history matching process.

Despite EnKF implementation to perform large scale reservoir history matching [5], there remain some unsolved problems. Most of the problems come from the internal linearity - Gaussianity assumptions from original Kalman filter. These are due to fact that most real dynamic systems follow nonlinear, non- Gaussian pattern. The former problem, itself, causes underestimation of variance by applying small ensemble size during data assimilation [6]. Often, these problems lead to filter divergence; in some cases ensemble members collapse to single estimate or the results tend to deviate from the true one as more data assimilated.

Since EnKF is a Monte Carlo implementation of Kalman filter, in practical applications it is limited to small ensemble size due to computational limitations. Use of ensemble with small size leads to appearance of spurious correlations in estimated cross-covariance matrices required for assimilation while in reality these correlation doesn't exist [7]. Wrong correlations between entries of covariance matrices causes incorrect state vector update, resulting underrate posterior state covariance estimation. Repeating the assimilation cycles with such behaviors rapidly diminishes ensemble variance toward zero [4].

One readily approach to cope with the aforementioned problems is to use of a large ensemble set but

unfortunately, this requires a high computational time. The number of unknowns (both parameters and states) in the geological and flow models, four or more parameters/variables per grid block and the huge number of simulation grid blocks prevents the use of large ensemble size. Therefore, motivation is raised to use any rational paradigm to do history matching efficiently by the use of small size ensembles.

Multiplying estimated state error covariance matrix elementwise with a locally supported correlation matrix yields an approach to overcome the small ensemble effects to some extent [4]. This approach known as covariance localization assumes that states beyond a specific distance from observation location are affected lesser by that observation. In the first application of covariance localization, a cut off radius was applied to assimilate observation just within circle formed by the radius [8]. Following [8], the authors developed a distance dependent localization approach [9] that employs a spatial correlation function with compact support to form localization matrix to filter out incorrect estimated covariance. With emphasis on the importance of covariance localization, this idea becomes a great deal of research. Several other methods, also, have been presented in order to cope with various aspect of localization which has their own merits and demerits [10-13].

In this work, it is aimed to investigate and compare various distance dependent correlation function which are employed to build localization matrix by comparing the ability and behavior of spatial distance dependent correlation function in the oil reservoir history matching. Here, we compared five different common correlation functions [14], namely, fifth-order correlation function (FIF), Third Order Autoregressive (TOA) function, exponential function (EXP), Second Order Autoregressive (SOA) Function and quartic function (QUA) to investigate their superiority.

This work is organized as follow; in this section, we present the EnKF formulation in history matching framework. Then the covariance localization along with correlation functions are described. Results of various correlation functions during history matching on two different test cases; a linear 2D static model and a 2D two-phase oil-water flow case, are presented along with a discussion subsection. Finally, we summarized our finding in conclusion.

ENSEMBLE KALMAN FILTER FOR HISTORY MATCHING

Let x and d be a state vector of size $n \times 1$ and observation/measuring data of size $d \times 1$ in which their time propagation follows a Linear Time-Varying (LTV) model dynamic with white Gaussian model noise w and white Gaussian measurement noise v :

$$x_t = M_t x_{t-1} + w_t \quad (1)$$

$$d_t = H_t x_t + v_t \quad (2)$$

Here, matrix M and H are model propagator and observation operator, respectively. It should be noted that there is no external input explicitly in the model. Indeed, it has been assumed that the reservoir is under normal operation (no change in production/injection flow rate) or is operating in a closed loop manner with no change in setpoints. We will drop subscript time t for the sake of easy development. The well known Kalman Filter (KF) optimally calculates the analysis state x^a (posteriori or updated estimate) through integration of model dynamic forecast x^f (prior forecast) of Eq.(1) with measurements coming from real system as:

$$x^a = x^f + K(d - Hx^f) \quad (3)$$

$$P^a = (I - KH)P^f \quad (4)$$

Here, matrix P of size $n \times n$ is state error covariance and subscripts f and a representing forecast and analysis and K is Kalman gain of size $n \times d$ which is obtained as:

$$K = P^f H^T (HP^f H^T + R)^{-1} \quad (5)$$

Here T is matrix transpose and R of size $d \times d$ represent observation error covariance matrix [15]. For large scale systems the propagation and storage of covariance matrices is not feasible and often impossible. Aside from this, real systems are nonlinear both in model and observation dynamic equations. These facts suggest incapability of KF for such systems. Evensen proposed a Monte Carlo implementation of KF [16]. In Ensemble Kalman Filter (EnKF) Probability Density Function (PDF) of the state vector is represented by a finite N_e number of randomly generated realizations $x_i (i=1,2,\dots,N_e)$ of system initial PDF. The ensemble set carries both state and state error covariance through propagation and updating of

each member. Here, x_i is an ensemble member of equal dimension of state vector. The estimate of state vector is the mean of ensemble set as the best estimate of states:

$$\bar{x} = \frac{1}{N} \sum_{i=1}^N x_i \quad (6)$$

And the required covariance matrix can be easily obtained from the ensemble set as:

$$P = \frac{1}{N-1} \sum_{i=1}^N (x_i - \bar{x})(x_i - \bar{x})^T \quad (7)$$

The EnKF procedure can be described as follow. At first, N_e realizations are generated from initial state vector x_0 and its associated error covariance matrix P_0 . All of generated realizations are then propagated with nonlinear model dynamic equation F (in our case a reservoir simulator) until a new observation becomes available (first step of data assimilation or prediction step):

$$x_i^f = F(x_i^a, v) \quad i = 1, \dots, N_e \quad (8)$$

Note that Eq. (8) is used for nonlinear forecasting of states instead of LTV equation (1). With measurement data and forecasted realizations being available, all requirement to perform calculations in Eq.(3) are provided:

$$x_i^a = x_i^f + K(d_i - Hx_i^f) \quad i = 1, \dots, N_e \quad (9)$$

After updating of all ensemble members are accomplished, these members are used as initialization of next assimilation cycle.

Some researchers have proven that utilizing the single obtained measurement d from real system in assimilation procedure results in analysis error covariance P^a being $(I - KH)P^f (KH)^T$ value less than of the value given by Kalman filter theoretical equation, Eq.(4), [17,18]. By performing assimilation using measurement d successively, most of ensemble member collapse to a single realization causing filter divergence. To avoid such divergence, they proposed applying a realization of measurement vector $d_i (i=1,\dots,N_e)$ instead of employing d straightforward in assimilation process. Here, d_i is a perturbed observation, which is computed with addition of random error with mean zero and covariance matrix equal to measurement covariance to real observation d .

To perform petroleum reservoir history matching, at first it is required to generate an ensemble of reservoir that follows unknown reservoir geostatistical model. Next, all members should be propagated with a reservoir simulator to next measurement time. With observation availability and computation of Kalman gain, someone can condition ensemble set to new data with EnKF as described above. The whole procedure is repeated if there is more observation. In this case, the state vector x is defined to contain states of system (pressure and saturations of present fluid phases in the reservoir), and parameters of system (natural logarithm of permeability). Hence, the augmented states are defined as $x_i = (p_i, s_i, \ln k_i)^T$. p_i , s_i , and $\ln k_i$ are pressure, saturation, and log-permeability of i^{th} realization, respectively.

COVARIANCE LOCALIZATION

As it is stated before, in practice, EnKF implementation is limited to small ensemble size. Working with small number of realizations introduces sampling error and causes inappropriate covariance propagation in ensemble members. To mitigate this problem and increasing the effective ensemble size (without actually using higher ensemble number) the covariance localization is proposed [8]. There are currently some different techniques for covariance localization [11, 12, 21]; but we will use the distance dependent types of localization techniques. In this method, instead of applying forecast error covariance matrix P^f directly to update ensemble set, it is replaced with its scaled version, the localized covariance matrix:

$$\hat{P}^f = \rho \circ P^f \quad (10)$$

This correlation matrix provides more weight to the points near observations than points far away in a region defined by critical length do . Matrix ρ is known as localization matrix (or sometimes correlation matrix) which is positive definite and the operator \circ indicates the Schur product which is element-wise matrix multiplication. In [4], authors discussed that due to Schur product properties the rank of localized covariance matrix \hat{P}^f is larger than original covariance leading to more stable EnKF performance. *Gaspari & Cohn* [14] provided some criteria that such a matrix should fulfill. They also provided some functions which produce such

correlation matrix. Here we will bring five of the recommended functions to apply in history matching problem. To see the descriptions and properties of following functions see [14]. r is physical distance between any state point to another one in all state vector entry point.

1- Fifth-order correlation function (FIF)

$$\rho(r) = \begin{cases} -\frac{r^5}{4} + \frac{r^4}{2} + \frac{5r^3}{8} - \frac{5r^2}{3} + 1 & 0 \leq r \leq 1 \\ +\frac{r^5}{12} - \frac{r^4}{2} + \frac{5r^3}{8} + \frac{5r^2}{3} - 5r + 4 - \frac{2}{3r} & 1 \leq r \leq 2 \\ 0 & 2 \leq r \end{cases} \quad (11)$$

2- Third order autoregressive function (TOA)

$$\rho(r) = (1 + r + r^2 / 3) \exp(-r) \quad (12)$$

3- Exponential Function (EXP)

$$\rho(r) = \exp(-0.5r^3) \quad (13)$$

4- Second order autoregressive function (SOA)

$$\rho(r) = (1 + r) \exp(-r) \quad (14)$$

5- Quartic function (QUA)

$$\rho(r) = \begin{cases} (1 - r^4)^4 & r \leq 1 \\ 0 & r > 1 \end{cases} \quad (15)$$

In fact, r is a dimensionless length which is calculated by dividing actual Euclidian length between any two points of state vector to a critical correlation length L_c . The critical length represents the maximum correlation lengths in a systems in which beyond of it correlation is zero or negligible. There is another correlation function, Gaussian, that is much suited for but its properties are similar to the fifth-order correlation function, so it is not considered here. The behaviors of correlation functions with dimensionless length are displayed in Fig. 1. As it can be observed third and second order autoregressive correlation functions have the most extreme behaviors after dimensionless $r=1$ meanwhile others rapidly decrease after this distance. QUA function seems has an interesting behavior; it reach to zero just before $r=1$.

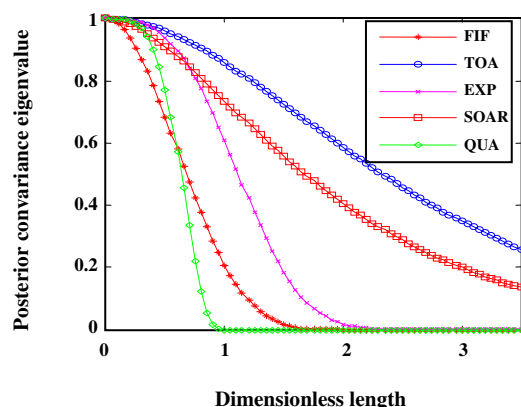


Fig. 1: Correlation functions behavior with dimensionless length.

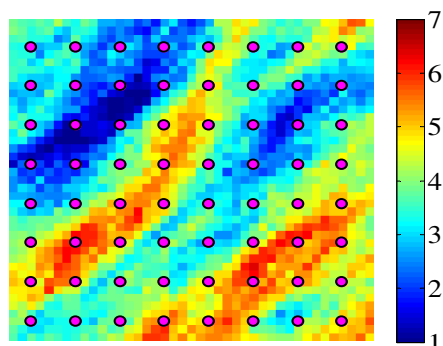


Fig. 2: True permeability field of test case one and measurement location (red circle). Note: in all figures, the legend shows the logarithm of permeability.

EXPERIMENTAL SETTING

Test case 1: 2D linear model

For this test, we consider an unreal 2D linear permeability model. The model is a synthetic 2D reservoir with size of 41×41 uniform grid blocks, totally 1681 grid blocks permeability to be estimated. To perform the EnKF, realizations of reservoir are acquired through the so-called sampling process. For this, the true permeability model (Fig. 2) is generated with an anisotropic spherical covariance with major correlation range of 20 grid blocks and minor correlation range of 8 grid blocks. The major correlation length is oriented along 45 degree anticlockwise from x-axis coordinate. The permeability model generation is performed applying sequential Gaussian simulation module of SGeMS [22] without any hard data conditioning. The prior log-

permeability mean and variance are 4 and 1, respectively.

Ensemble set is also generated using the true model procedure and its covariance. To obtain observation data, it is supposed that measurements are directly available from true reservoir model with a measurement error. The error is a white Gaussian noise with zero mean and standard deviation of five mD. The filled circles in Fig. 2 represent the measurement location, totally 64 data point. It should be noted that true model is just an unknown model that should be obtained by applying the data assimilation from measurement data.

For this linear case, we can compare the results of EnKF with best possible solution obtained by Maximum A Posterior (MAP) method [19]. This solution for linear Gaussian dynamic in Bayesian integration framework is obtained by minimizing following objective function:

$$2O(m) = 2O_m(m) + 2O_d(m) = \quad (16)$$

$$(m - m_p)^T C_m^{-1} (m - m_p) + (Hm - d)^T C_d^{-1} (Hm - d)$$

m contains the reservoir parameters (here log-permeability of reservoir grid blocks) and m_p is prior knowledge of the parameters. C_m and C_d are covariance matrix of the parameters and measurements, respectively. By analytical minimizing of Eq.(16), MAP solution can be calculated:

$$m_{MAP} = m_p + C_m H^T (C_d + H C_m H^T)^{-1} (d - H m_p) \quad (17)$$

We will use the MAP solution to compare the EnKF results.

In this test case, the state vector in EnKF is just log-permeability values. We applied the EnKF procedure described in previous section to assimilate permeability measurement data accordingly, for two different ensemble set of 10 (set A) and 25 (set B) realizations. To compare the assimilation results with use of various localization functions for small ensemble, the MAP and large ensemble size posteriori are also calculated for.

Fig. 3 (left) depicts the prior ensemble mean of ensemble set A which is going to be used for assimilation process latter. In the center of this figure, the MAP estimation from applying ensemble set A and measurement data is displayed. And finally, the mean of EnKF estimation without localization utilizing 1000 realizations is shown in right part of Fig. 3.

Comparing Figs. 2 and 3 reveals that MAP and

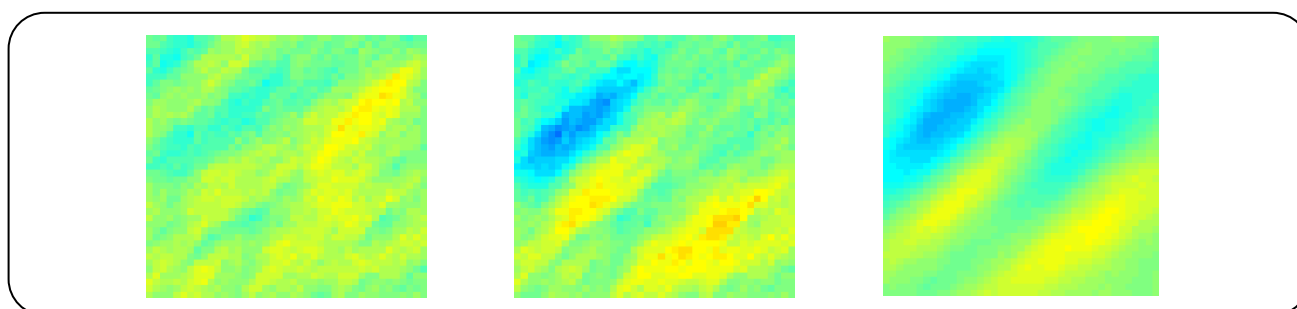


Fig. 3: Mean of ensemble set A (left), MAP estimation for set A (center), mean of EnKF without localization for 1000 realizations.

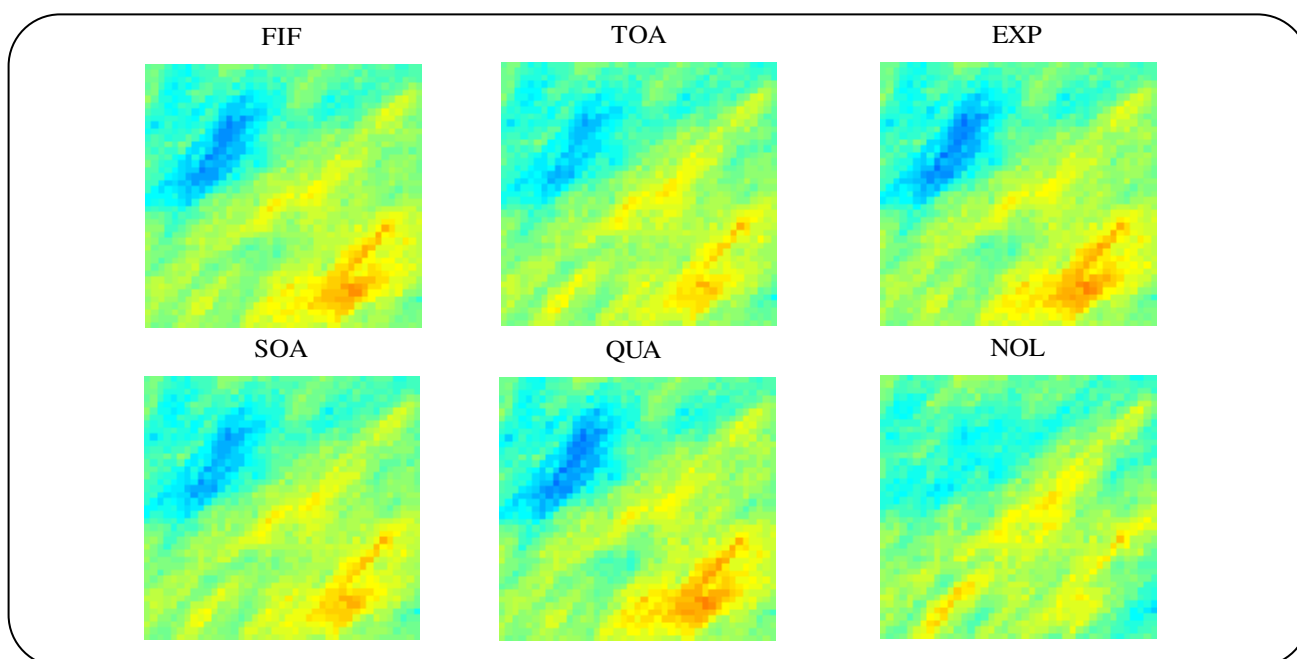


Fig. 4: Estimated permeability map for ensemble set A with different localization functions; NOL refers to no localization.

EnKF with large ensemble size estimated high (lower area in Fig. 2) and low (upper area in Fig. 2) permeability regions (high-low permeability features) of true model quite similarly but still MAP estimate is better.

The localization functions described in previous section are employed within EnKF to estimate permeability of true model with critical length equal to 15 grid blocks. We should point out that this number is obtained by trial and error. Fig. 4 represents the estimated permeability map by employing various localization functions and EnKF for ensemble set A. The case without localization is also presented for comparison. It is obvious that fifth order, exponential and quartic correlation functions have produced nearly similar results and much better than autoregressive variants. In addition, provided permeability

map of all localization functions is much better than no localization case within the same assimilation procedure. Especially, low-high permeability strikes are almost never characterized in the NOL (no localization function) case.

Similar to ensemble set A, the whole process was repeated for ensemble set B to see the effect of larger ensemble size (25 realizations). In Fig. 5 similar results of Fig. 3 is presented. Increasing the ensemble number provides more prior information to MAP solution leading to more accurate permeability estimation than ensemble set A (compare middle Figs. 3 and 5).

Results of assimilation procedure for ensemble set B with and without localization are displayed in Fig. 6. With increasing ensemble size, estimated permeability map of all localization functions but spherical are similar

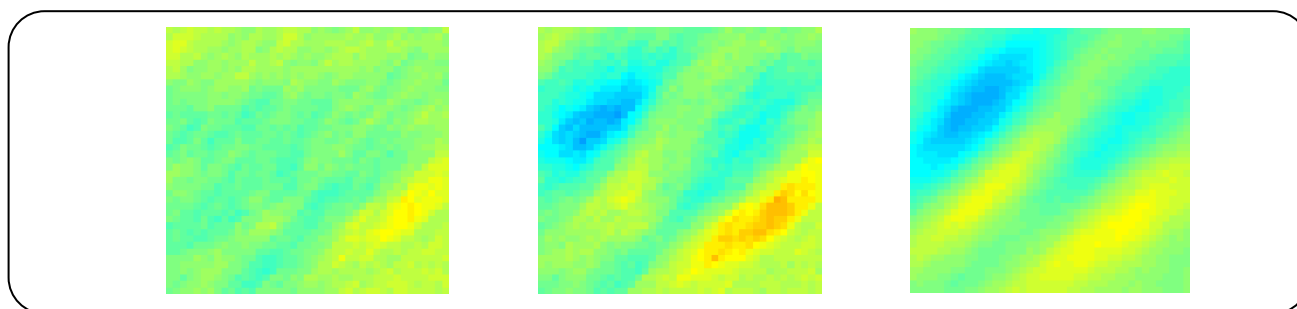


Fig. 5: Mean of ensemble set B (left), MAP estimation for set B (center), mean of EnKF without localization for 1000 realizations.

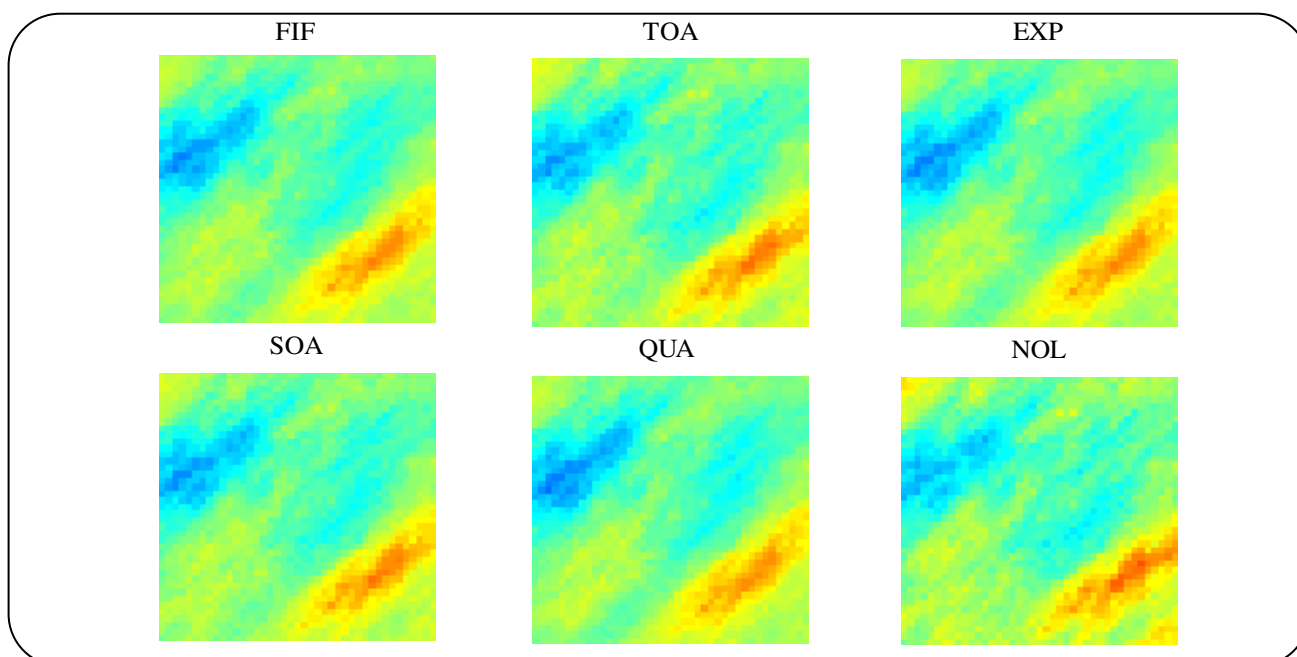


Fig. 6: Estimated permeability map for ensemble set B with different localization functions, NOL refers to no localization.

and again better than no localization case. There are some tools to evaluate the performance of localization. In order to investigate the effect of localization on assimilation results, eigenvalues of posterior permeability covariance for each localization function and for two ensemble set are calculated and results are presented in Fig. 7. In this figure, the y-axis represents the values of eigenvalues in descending order

There are some interesting points that can be observed from Fig. 7. At first, for both ensemble set A and B, the eigenvalues of no localization case are smaller than any of with localization cases. Increasing the ensemble size increases the number of nonzero eigenvalues which provides higher rank for posterior covariance. The eigenvalues range comes closer for larger ensemble set meaning the importance of all of

Eigen mode of the system simultaneously. The TOA and SOA have similar eigenvalues and those values are smaller than other localization function. This can quite fairly explain the better results obtained for FIF, EXP and QUA relative to TOA and SOA earlier.

To see the effect of critical correlation length on the history matching results, results of data assimilation of ensemble set B for critical length equal to 4 and 20 grid blocks are presented in figure 8 and 9, respectively.

From Figs. 8 and 9 the importance of critical length correct selection is revealed. Choosing inappropriate critical length for all localization functions have severe drawback on assimilated results. It is notable that TOA and SOA are more robust on critical length value than other localization functions as can be seen from Figs. 6, 8 and 9.

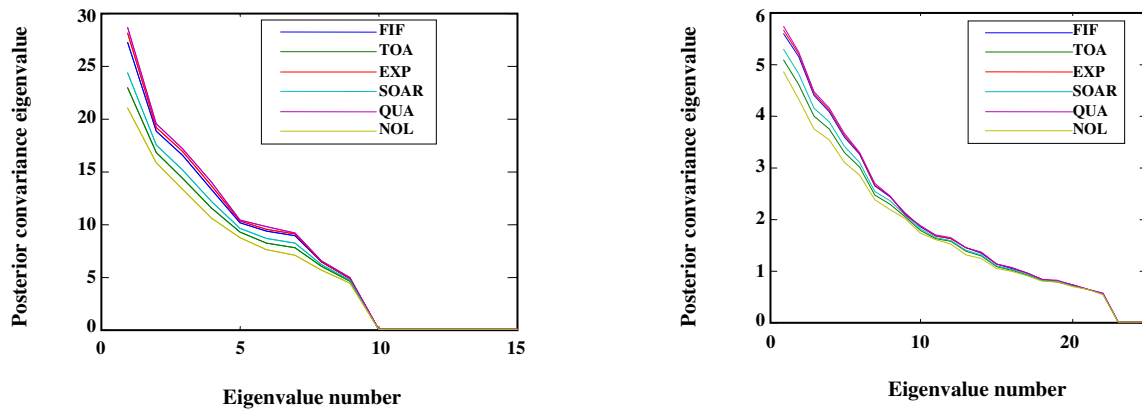


Fig. 7: Eigenvalues of posterior permeability covariance for both ensemble set and each localization functions.

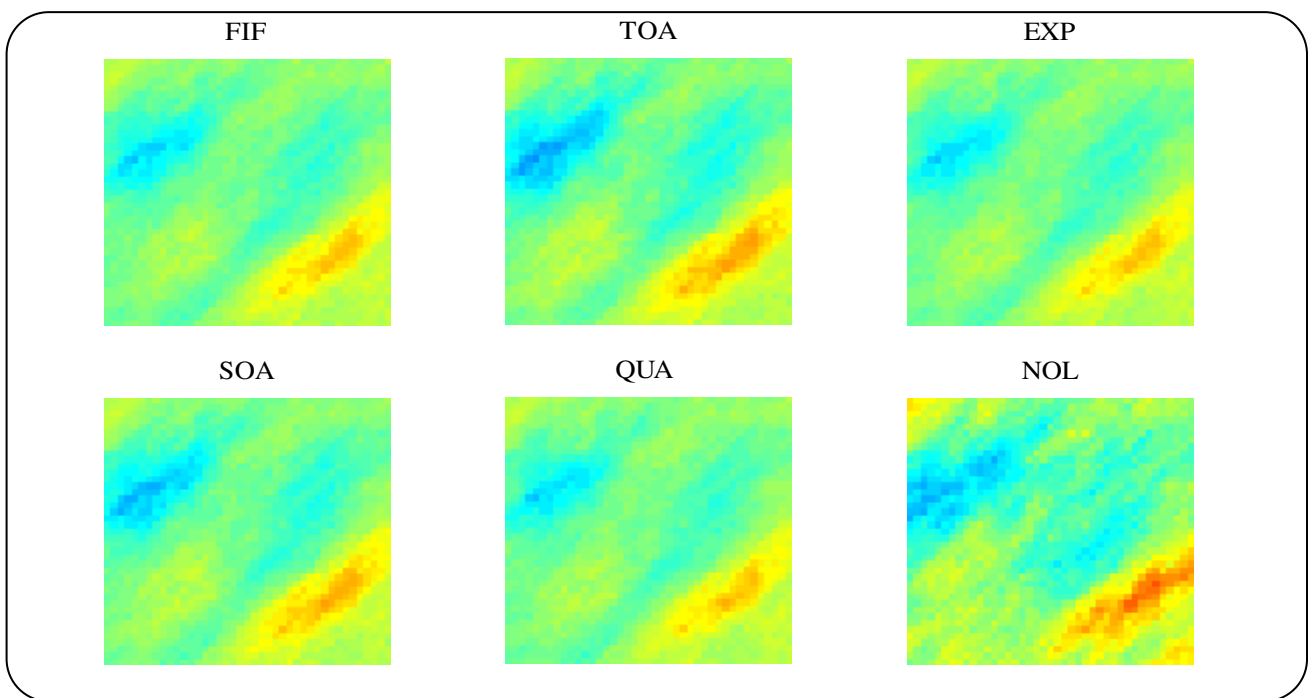


Fig. 8: Estimated permeability for ensemble set B with critical length 4 grid blocks.

Test case 2: 2D nonlinear dynamic

For this test case, history matching of a two dimensional – two phases oil - water flow synthetic reservoir was considered. The reference model of test case 1 is employed here as true permeability field to generate measured production data. The dimension of each grid block is fixed as $40 \times 40 \times 10$ ft. An inverted five spot water flooding well pattern is established: a water injector in the center of 2D reservoir and four producers at four corners of it. Water is injected with constant rate of 500 STB/D. All producers have constant bottomhole

pressure set at 3000 psi. Table 1 presents the summary data of the water-flooding pattern.

Initial reservoir oil pressure and connate water saturation are 3000 psi and 0.2, respectively. Grid block porosity is fixed to 20 %. True permeability field is employed to generate the reference production data. Production data set consist of injection well bottomhole pressure and oil - water production rates from producers; totally 9 data for each assimilation cycle. Production data are obtained every 2 months for three years of reservoir production providing 18 assimilation cycles. The “true”

Table 1: Summary of the well patterns for test case 2.

Well	Inj	P1	P2	P3	P4
Well type	Injector	Producer	Producer	Producer	Producer
x location	21	5	5	36	36
y location	21	5	36	5	36
Constraints	500 STB/D	3000 psi	3000 psi	3000 psi	3000 psi

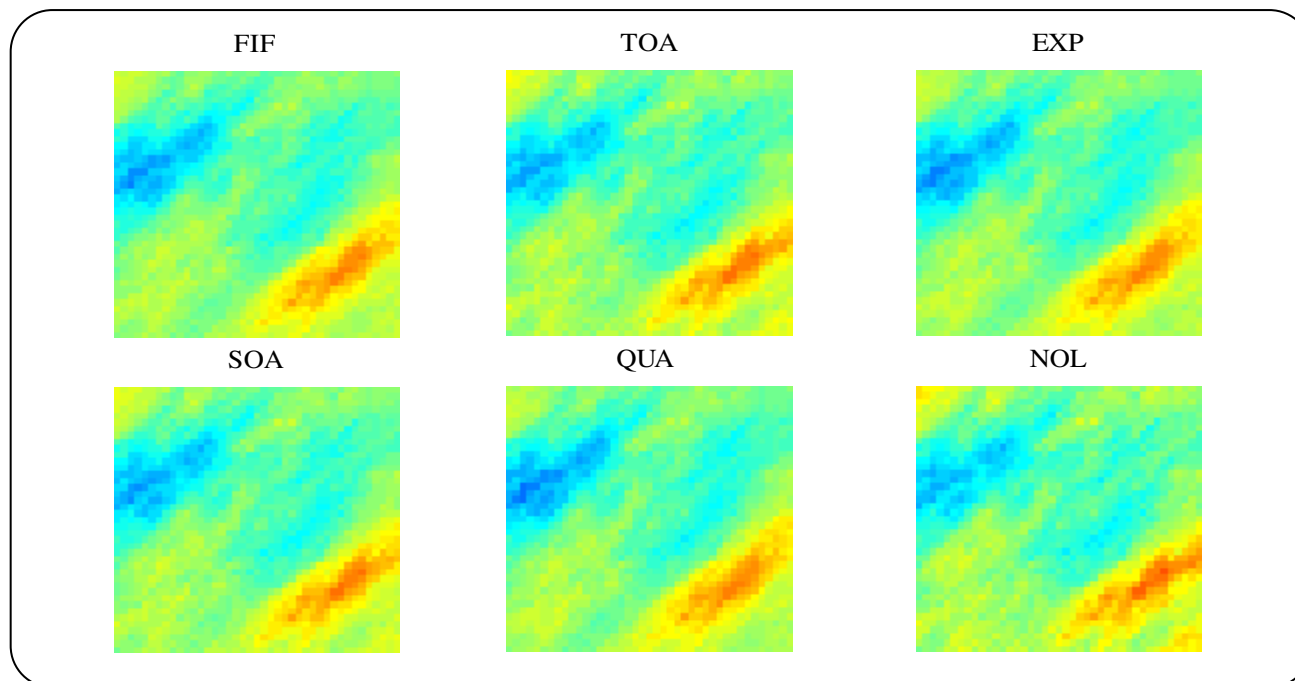


Fig. 9: Estimated permeability for ensemble set B with critical length 20 grid blocks.

production data are then perturbed with a white Gaussian noise with mean zero and standard deviation of 8 psi and 4 STB/D for bottomhole pressure and production rate, respectively, to emulate noisy measurement data. True and noisy production data are plotted in Fig. 10. It is worth to emphasize that the reason this model was selected for case 2 is that it has strong heterogeneity within. This leads to a more challenging problem and a better test case to compare correlation functions.

To evaluate filter performance two different criteria are applied: Root Mean Square Error (RMSE) and ensemble spread. A convergence of assimilation process will yield diminishing of both RMSE and spread along time. These criteria are defined in Eq. (18) and (19), respectively [23].

$$\text{rmse}_i = \sqrt{\frac{1}{N_e} \sum_{j=1}^{N_e} (x_{j,i} - x_i^t)^2} \quad i = 1, \dots, N \quad (18)$$

Here x is natural logarithm of permeability, x^t represents true permeability in case of twin experiment and N is the total number of estimated parameters.

$$\sigma_i = \sqrt{\frac{1}{N_e} \sum_{j=1}^{N_e} (x_{j,i} - \bar{x}_i)^2} \quad i = 1, \dots, N \quad (19)$$

In this formula \bar{x} is mean of estimated ensemble. It should be pointed out that to obtain a scalar value of RMSE and spread at any time someone required to calculate an average over all grid blocks.

The history matching process is performed as described in section 2. The results of applying localization with critical length equal to 30 grid blocks for three different ensemble sizes 25, 50 and 100 member are depicted through Figs. 11, 12, 13, respectively in the same uniform scale.

Ensemble set with size 25 members is almost

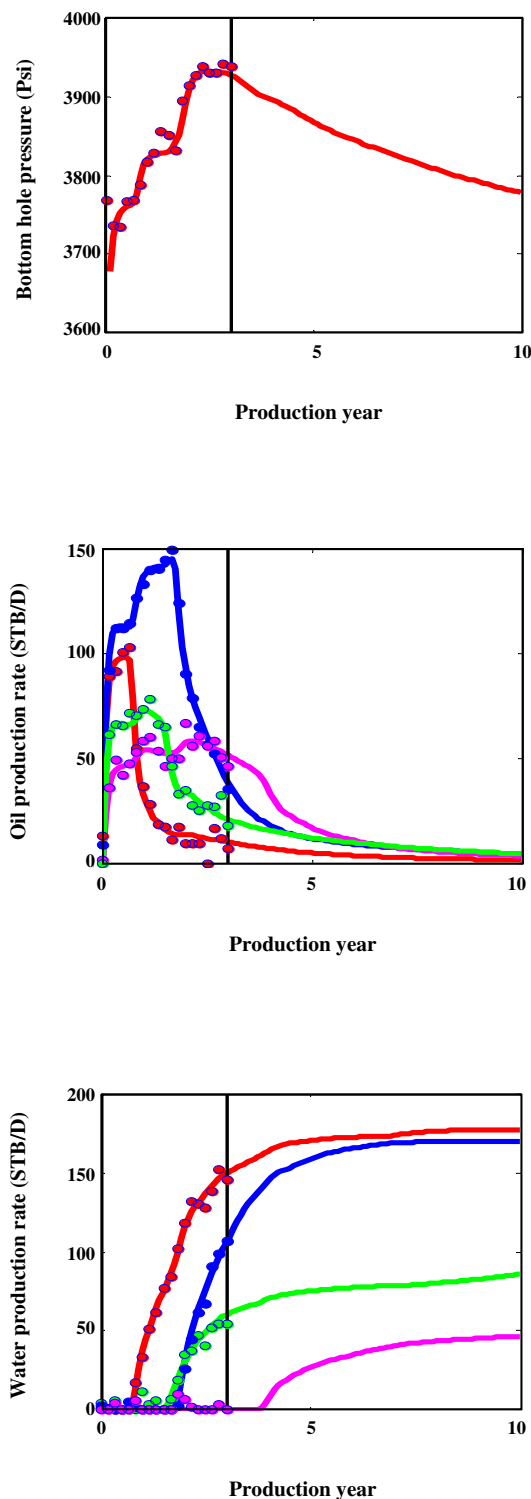


Fig. 10: plot of production data, injection pressure (up), oil and water production rates (middle and down), the circles show noisy observation, and solid lines are true production. Color represents different well.

incapable to recover the main trend in reference map. Estimated map in this case is not only far from true but also represents severe overshooting (values too much greater than the maximum value in reference map) in estimated permeability. Although, results of QUA/FIF function are better from other ones and display less overshooting.

For case with 50 realizations (Fig. 12) results are better than the aforementioned one with much lower overshooting values. But still, noisiness in characterized maps is lucid. Among the correlation functions, QUA/FIF are able to retrieve some of the main features and trends in true case. A notable recovered trend of QUA that all other correlation functions yet failed to identify, is the top-left low permeability curvilinear strike in the true map.

Finally, in Fig. 13 the estimated permeability map for the 19th assimilation period is depicted. The first idea comes from this figure is the smoothness of estimated localized map of FIF/QUA relative to NOL and other functions. This property, also, occurs in Figs. 11 and 12 but here it is much more obvious. Here, QUA and FIF results are very similar in part similar to true.

The RMSE and spread of localization functions with different critical lengths and ensemble sizes are computed and plotted in Figs. 14 and 15, respectively. In both figure 14 and 15, each row is for a specific ensemble size: 25, 50, and 100 from top row to bottom. Each column represents a particular critical length: from left to right 5, 15 and 30 grid blocks in order.

As it is clear from RMSE equation, smaller RMSE dedicates closer estimation to true permeability values. This implies that as assimilation progress in time it would be natural to obtain smaller RMSE. However, as it can be observed from Fig. 14 (black line), regardless of ensemble size, RMSE of no-localization case (i.e. pure EnKF) follows either an oscillatory trend (case $N_e = 100$) or diminishing-increasing trends (case $N_e = 25/50$). In other word, EnKF alone cannot recover the true permeability map by assimilation of production data.

The reason for such behavior against our intuition is a research topic and we are not going into it. But the localization procedure attempts to mitigate the problem. Interesting point is that increasing the critical length lead to no-localization case performance. As can be seen in Fig. 14, for different localization function different optimal critical length is required.

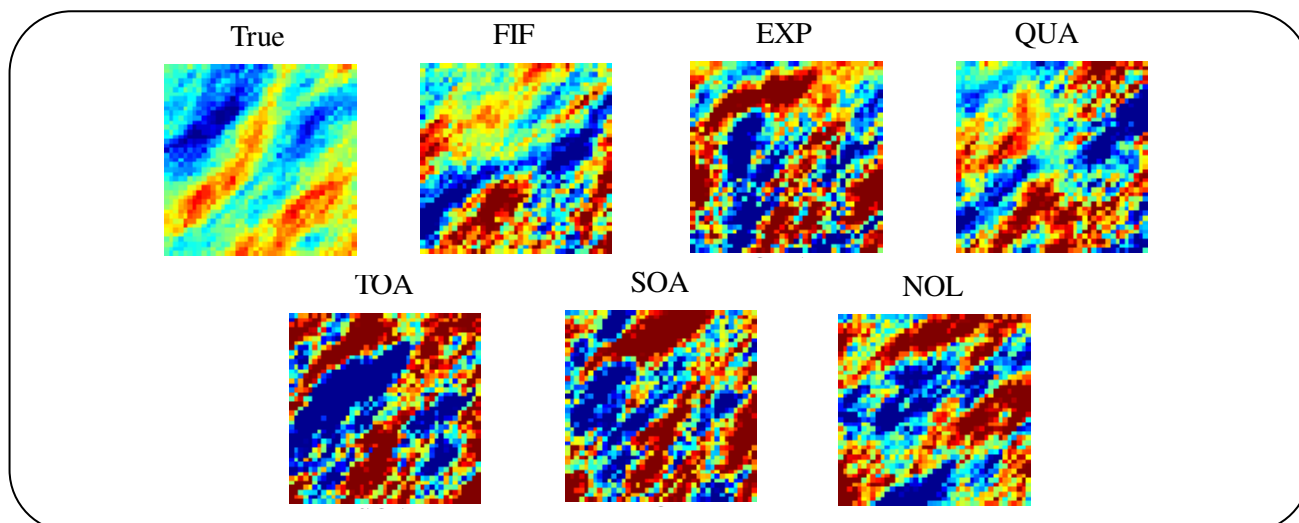


Fig. 11: Estimated permeability for $N_e = 25$ with critical length 30 grid blocks for the last assimilation cycle.

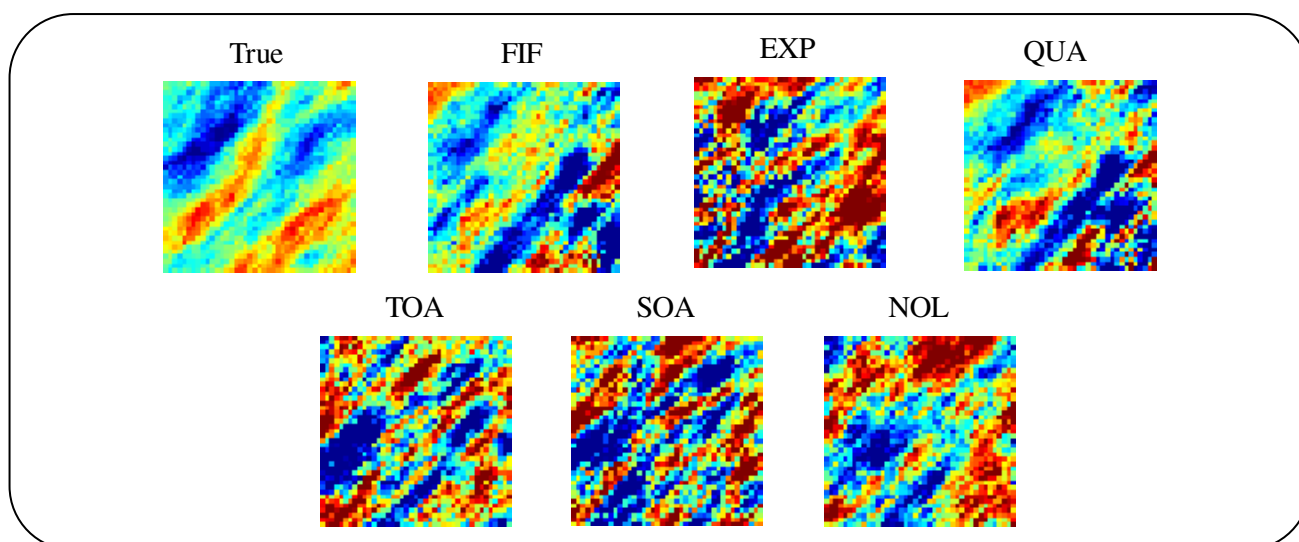


Fig. 12: Estimated permeability for $N_e = 50$ with critical length 30 grid blocks for the last assimilation cycle.

Another point is that for small critical length the QUA, FIF and EXP provide more robust performance but slowly decreasing RMSE than other two functions. For medium critical length QUA and EXP display a more robust one. Finally, for large critical value, the performance of localization approaches to no-localization case results. As ensemble size grows, for small critical length value, SOA produces best diminishing RMSE with a robust trend and for medium one; EXP, QUA and FIF produce diminishing RMSE with a robust trend.

Fig. 14 confirms previous stated conclusion [9] on critical length value in distance-based localization that was used for state estimation; here instead for parameter

estimation: As the ensemble size grows (25, 50 and 100) the optimal critical value to perform better results increase.

It is notable to point out that spread represents the total variance in each component of state vector. And the scalar value calculated and displayed in Fig. 15 is the total variance of all members for all grid blocks permeability. So as it is clear in Fig. 15, as data are integrated into realizations, the total variance of system decrease. This is something that our intuition states. The interesting point is that regardless of localization functions or critical lengths, the total variance of localized cases are greater than no-localization case

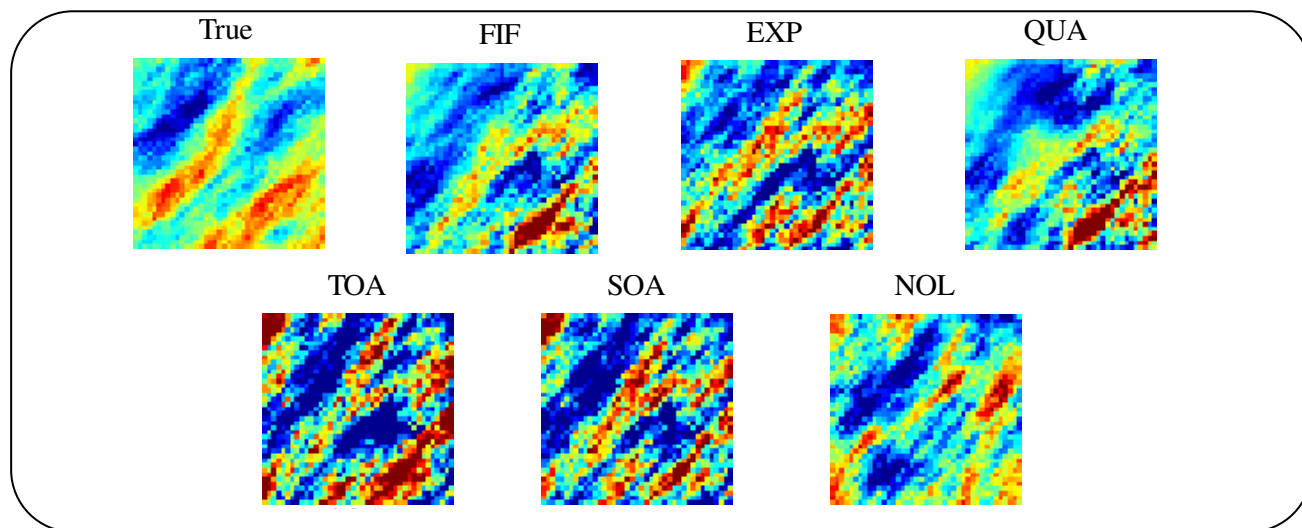


Fig. 13: Estimated permeability for $N_e = 100$ with critical length 30 grid blocks for the last assimilation cycle.

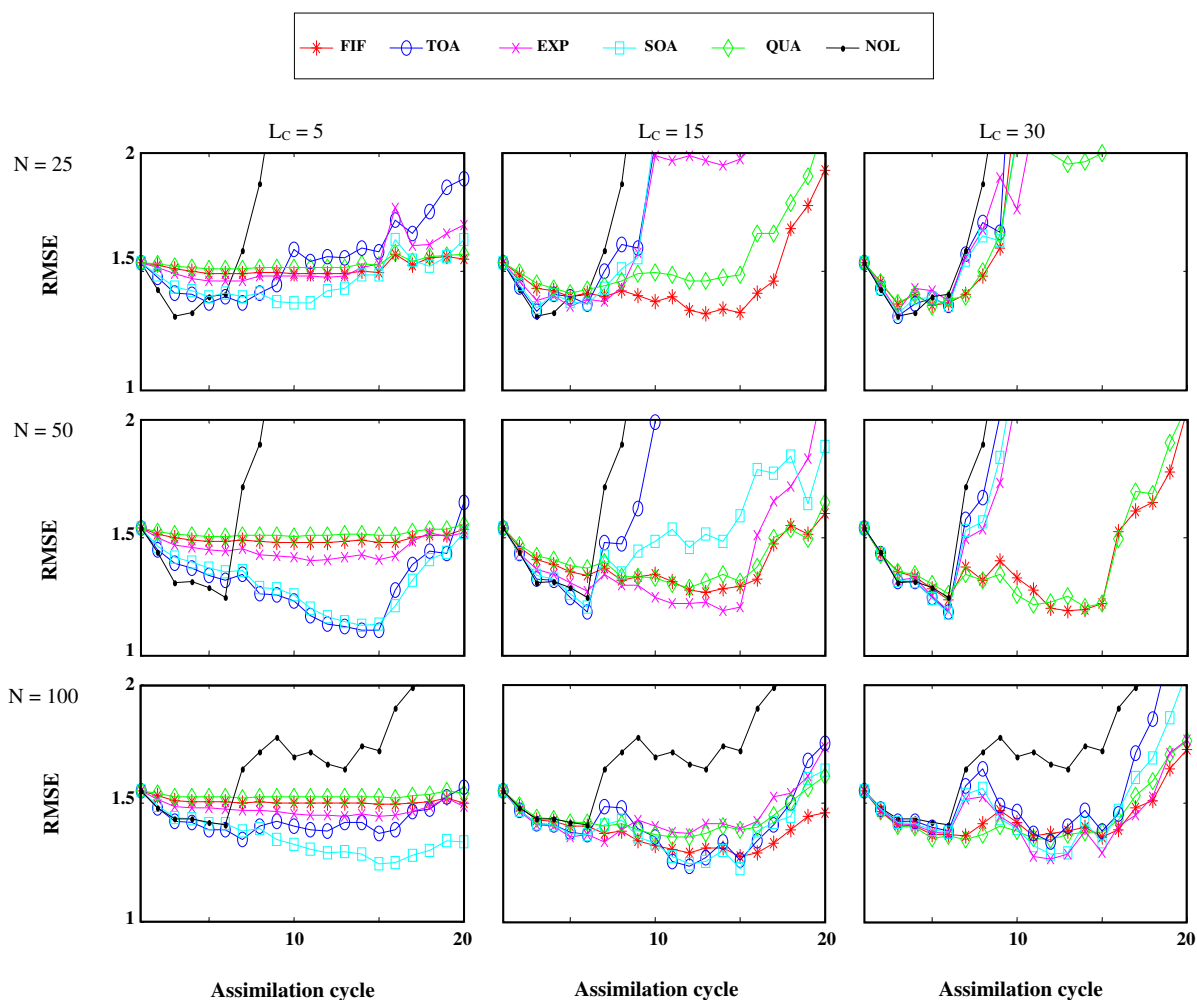


Fig. 14: Plot of root mean square error (RMSE). From top to bottom, ensemble size for each row is 25, 50 and 100. From left to right critical lengths are 5, 15 and 30 grid blocks. N is number of realizations.

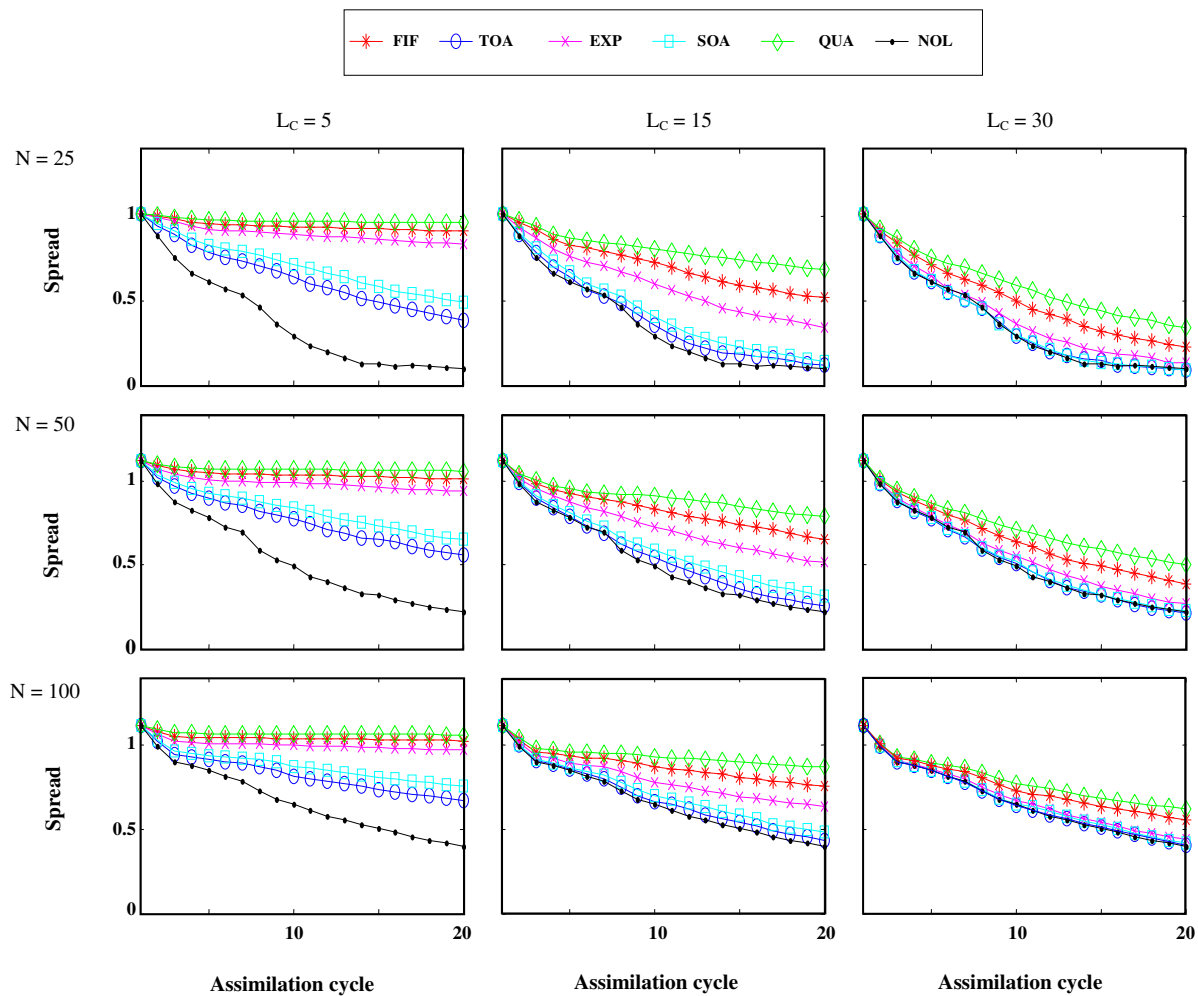


Fig. 15: Plot of spread. From top to bottom, ensemble size for each row is 25, 50 and 100. From left to right critical lengths are 5, 15 and 30 grid blocks. N is number of realizations.

no matter what. This was one of localization priority aim to maintain the variance of the system as far as possible. Another note from Fig. 15 is that although QUA and FIF functions maintain the largest total variance but QUA is the only function that outperform other functions in term of total variance in all cases presented in Fig. 15.

The uncertainty of predicted future production profile can be helpful to see even more on localization performance. To view this, the estimated permeability maps of all functions were utilized in a reservoir simulator and simulations were performed from time zeros to 10 years ahead. The results are tremendous amount of data for analysis.

We brought here data of oil and water production rates of well P3 for case 50 realizations with localization length of 15 grid blocks. Figs. 16 and 17 depict the true

oil and water production from reference permeability (circle), all realizations (curves), the mean of realizations map (star) and finally the vertical line dividing the figures into history matched part (left part) and predicted part (right one). The reason that well P3 is selected to present its simulation results is that no water rate of P3 was employed during assimilation process. This makes the P3 a good candidate for such purpose.

For every time step (along x-axis in Fig. 16 and Fig: 17), we define the uncertainty merely as envelops made around true production data. For history matched section, QUA and TOA provide relatively good encompass (Fig. 16), meaning true data is between the extreme blue lines (realization data), but this cannot be stated for NOL case as history never matched correctly (see NOL in Fig. 16 and 17).

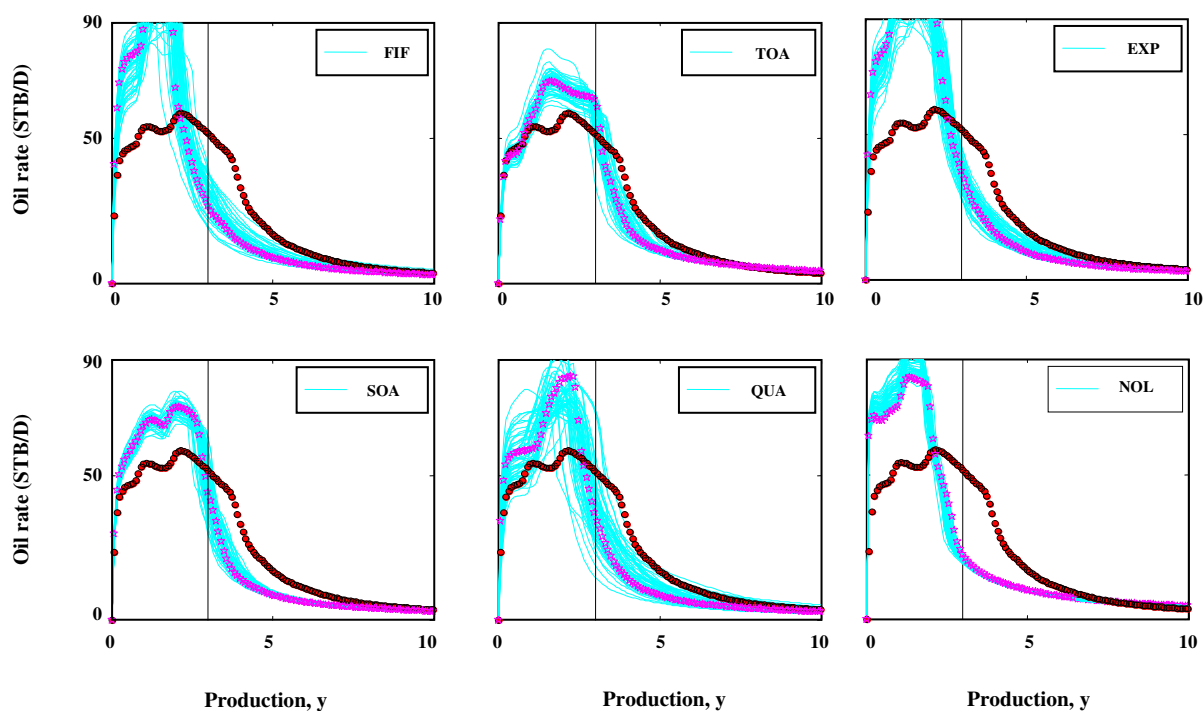


Fig. 16: Oil production profiles of well P3, True data (red circle), realizations (light blue), mean realizations map (magenta star), before /after vertical line: history and predicted production, x- axis: years of productions, y-axis: oil production rates STB/D.

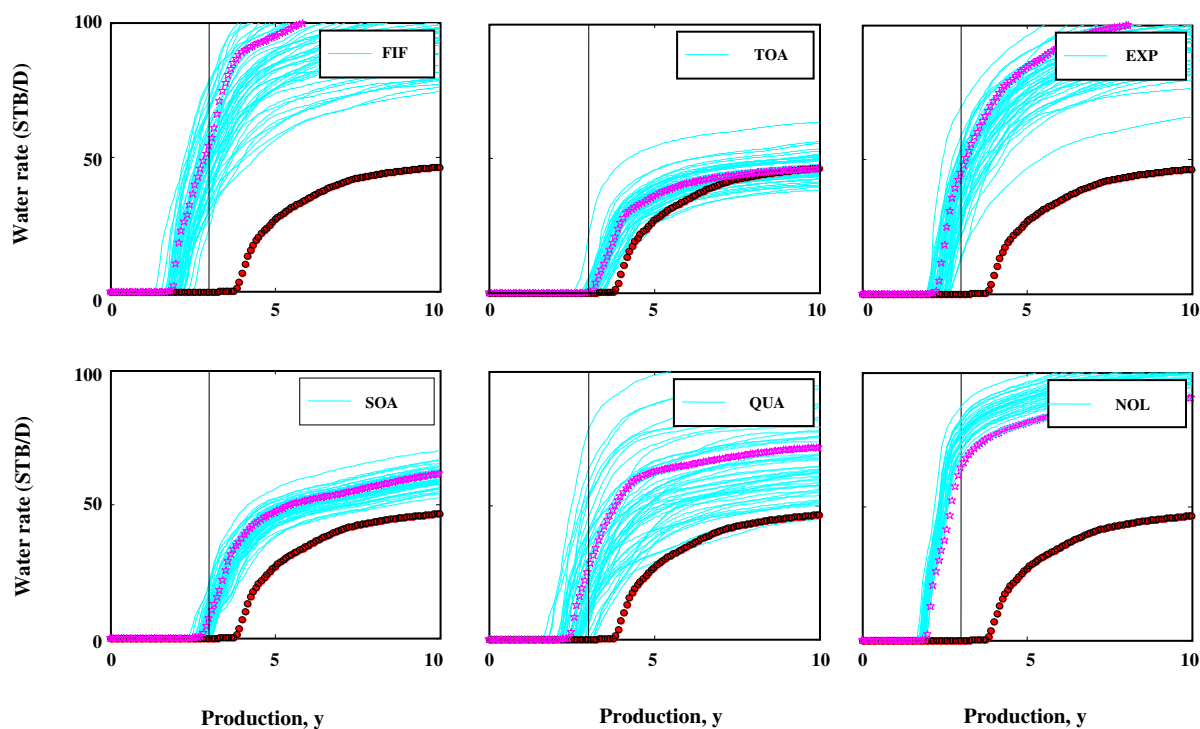


Fig. 17: Water production profiles of well P3, True data (red circle), realizations (light blue), mean realizations map (magenta star), before /after vertical line: history and predicted production, x- axis: years of productions, y-axis: water production rates STB/D.

Estimated uncertainty for prediction phase is quite notable for various localizations. Neither of the methods are able to recover the water breakthrough time and some part of water production rates and the estimated mean breakthrough is biased overly for all (Fig. 18). QUA and TOA functions have some members that encompass true water production.

DISCUSSION

We define any estimated permeability value greater than the highest/lowest permeability in the reference map as overshoot/undershoot. The common overshoot/undershoot is not a problem in history matching because this type of inverse problem cannot be solved uniquely [1]. It can be seen from figures 11 to 13 that, the localization process not only mitigates the overshooting problems (compare to NOL) but also attempt to avoid the overshooting as far as possible. It is also can be observed that in the NOL case, the estimated permeability map start to deteriorate very soon with more assimilation performed (as is depicted in RMSE values in Fig. 14).

Results indicate that in case of no-localization with sufficient large ensemble size, the overall high-low permeability features in the reference map can be identified as early as possible in assimilation cycles. However, the estimated features tend to deteriorate as more assimilation performed. It is also verified that with more and more assimilation cycles, in no-localization case the estimate collapse to single mean estimate of whole domain defined by ensemble members. Although localization removes some information from cross-covariances during assimilation, causing later identification of high-low features, but inclines to carry out a more robust estimation.

Localization, at least the cases we studied here, forces the estimated permeability maps (or any other state vector values) to be smoother. This can lucidly be observed from comparison of no-localization and localization results.

It is obvious that as critical length increases toward domain boundaries and beyond, the estimated map results approach to no-localization results (see Fig. 14). This highlights one thing clearly: the importance of correct critical length employment. Harms caused by incorrect critical length to assimilation results suggest to implement distance based covariance localization more carefully, specially it would be better to not apply distance based localization in case of inappropriate

critical length estimation. Authors in [7] suggested a method to obtain critical length but require somehow use of streamline simulation and sensitivity calculations, which are not available easily. It is also interesting that as ensemble number increase the stable critical length for localization increases.

Results, both in test case 1 and 2, suggest that TOA and SOA correlation functions perform almost similarly, but for large ensemble size SOA run more robust results with smaller critical length, although not able to find the high-low profiles. Another notable point for these correlation functions is that they produce more similar results to no-localization case relative to others. This can be explained from Fig.1: these two functions remove less incorrect information from cross-covariances.

Although our survey in literatures indicates that the FIF correlation function has been applied for distance based localization most of time [4], [7], [11]. Our results, however, indicate that QUA is not only yield robust permeability estimation but identify the high-low permeability features and their positions more correctly without uncommon overshooting and yet maintaining more total variance at the end of assimilation. To confirm this see Fig 14, 15 and Fig. 12, 11 and 10. Of course, the topic demands more research with implementing the functions on more cases like real/fracture reservoirs [24].

CONCLUSIONS

A sequential EnKF was developed to perform the history matching of reservoir model. To mitigate the spurious correlation effect on covariance due to small ensemble size, a distance base localization is employed. To investigate the behavior of different correlation functions that are utilized for localization, a comparative study are accomplished. The procedure is evaluated on two different test cases, one linear-static and the other a nonlinear-dynamic case.

In terms of uncertainty estimation the overall localization results was quite superior to NOL and among themselves, the FIF and QUA produced similar results. Results indicate that QUA functions is equally likely applicable for history matching procedure and provides similar or better results relative to traditional popular FIF.

Nomenclatures

x	State vector of size $n \times 1$
d	Observation vector of size $d \times 1$
M	Model propagator operator

H	Observation operator
x^a	Analysis state vector
x^f	Forecast state vector
P	State error covariance matrix of size $n \times n$
\hat{P}	Localized state error covariance matrix
K	Kalman gain matrix of size $n \times d$
N_e	Number realizations
N	Total number of active grid block
x_i	i th realization
F	Nonlinear model dynamic
w	White Gaussian model noise
v	White Gaussian measurement noise
d_i	Perturbed observation vector
p_i	Pressure state vector of i th realization
s_i	Saturation state vector of i th realization
$\ln k_i$	Natural logarithm of permeability state vector of i th realization
d_i	Predicted data of i th realization
m	Reservoir parameters
m_p	Prior knowledge of the reservoir parameters
C_m	Covariance matrix of the parameters
C_d	Covariance matrix of measurements
r	Dimensionless length
L_c	Critical correlation length
ρ	Localization matrix
f	Forecast
a	Analysis
ft	Foot (here, length unit)
EnKF	Ensemble Kalman filter
PDF	Probability density function
FIF	Fifth order covariance function
TOA	Third order autoregressive covariance function
EXP	Exponential covariance function
SOA	Second order autoregressive covariance function
QUA	Quartic covariance function
NOL	No localization function
DEnKF	Deterministic ensemble Kalman filter
STB/D	Stock tank barrel per day

Received : Dec. 3, 2012 ; Accepted : Jan. 14, 2014

REFERENCES

- [1] Oliver N., Reynolds D.S., Liu A.C., "Inverse Theory for Petroleum Reservoir Characterization and History Matching", Cambridge University Press, Cambridge, UK, (2008).
- [2] Nævdal G., Mannseth T., Vefring E.H., Near-Well Reservoir Monitoring Through Ensemble Kalman Filter, in *SPE/DOE Improved Oil Recovery Symposium*, no. 1, p. SPE 75235, (2002).
- [3] Gu Y., Oliver D.S., History Matching of the PUNQ-S3 Reservoir Model Using the Ensemble Kalman Filter, *SPE journal*, **10**(2), p.217, (2005).
- [4] Aanonsen S., Nævdal G., Oliver D., Reynolds A., The Ensemble Kalman Filter in Reservoir Engineering-a Review, *SPE Journal*, **14**(3), p.393., (2009).
- [5] Bianco A., Cominelli A., Dovera L., Nævdal G., Valles B., History Matching and Production Forecast Uncertainty by Means of the Ensemble Kalman Filter: a Real Field Application, in *SPE Europe/EAGE Annual Conference*, (2007).
- [6] Zhang Y., Liu N., Oliver D.S., Ensemble Filter Methods with Perturbed Observations Applied to Nonlinear Problems, *Computational Geosciences*, **14**(2), p. 249 (2009).
- [7] Emerick A., Reynolds A.C., Combining Sensitivities and Pprior Information for Covariance Localization in the Ensemble Kalman Filter for Petroleum Reservoir Applications, *Computational Geosciences*, **15**(2), p. 251 (2011).
- [8] Houtekamer P.L., Mitchell H.L., Data Assimilation Using an Ensemble Kalman Filter Technique, *Monthly Weather Review*, **1969**, p. 796 (1998).
- [9] Houtekamer P., Mitchell H.L., A Sequential Ensemble Kalman Filter for Atmospheric Data Assimilation, *Monthly Weather Review*, **ii**, p. 123 (2001).
- [10] Sakov P., Bertino L., Relation Between Two Common Localisation Methods for the EnKF, *Computational Geosciences*, **15**(2), p. 225 (2010).
- [11] Arroyo E., Devegowda D., Datta-Gupta A., Streamline Assisted Ensemble Kalman Filter for Rapid and Continuous Reservoir Model Updating, *SPE Reservoir Evaluation & Engineering*, **11**(6), p. 1046 (2006).
- [12] Chen Y., Oliver D.S., Cross-Covariances and Localization for EnKF in Multiphase Flow Data Assimilation, *Computational Geosciences*, **14**(4), p. 579 (2009).
- [13] Furrer R., Bengtsson T., Estimation of High-Dimensional Prior and Posterior Covariance Matrices in Kalman Filter Variants, *Journal of Multivariate Analysis*, **98**(2), p. 227 (2007).

- [14] Gaspari G., Cohn S.E., Construction of Correlation Functions in Two and Three Dimensions, *Quarterly Journal of the Royal Meteorological Society*, **125**(554), p. 723 (1999).
- [15] Evensen G., "Data assimilation: The Ensemble Kalman Filter", Springer, p. 330 (2009).
- [16] Evensen G., Sequential Data Assimilation with a Nonlinear Quasi-Geostrophic Model Using Monte Carlo Methods to Forecast Error Statistics, *Journal of Geophysical Research*, **99**(C5), p. 10143 (1994).
- [17] Burgers G., van Leeuwen P.J., Evensen G., Analysis Scheme in the Ensemble Kalman Filter, *Monthly Weather*, **126**(6), p. 1719 (1998).
- [18] Sakov P., Oke P.R., A Deterministic Formulation of the Ensemble Kalman Filter: An Alternative to Ensemble Square Root Filters, *Tellus A*, **60**(2), p. 361 (2008).
- [19] Zafari M., Reynolds A.C., Assessing the Uncertainty in Reservoir Description and Performance Predictions with the Ensemble Kalman Filter, *SPE Annual Technical Conference, SPE 95750* (2005).
- [20] Devegowda D., Arroyo E., Datta-Gupta A., Efficient and Robust Reservoir Model Updating Using Ensemble Kalman Filter with Sensitivity-Based Covariance Localization, *SPE Reservoir Simulation Symposium, SPE 106144* (2007).
- [21] Anderson J.L., Exploring the Need for Localization in Ensemble Data Assimilation Using a Hierarchical Ensemble Filter, *Physica D: Nonlinear Phenomena*, **230**(1–2), p. 99 (2007).
- [22] Remy N., Boucher A., Wu J., "Applied Geostatistics with SGeMS: A User's Guide", Cambridge University Press, p. 284 (2009).
- [23] Gu Y., Oliver D.S., The Ensemble Kalman Filter for Continuous Updating of Reservoir Simulation Models, *Journal of Energy Resources Technology*, **128**(1), p. 79 (2006).
- [24] Riazi Z., Rashidi F., Sensitivity Analysis of Cumulative Oil Production and Production Rate on Block Heights and Capillary Continuity for an Iranian Carbonated Fractured Reservoir, *Iran. J. Chem. Chem. Eng.*, **28**(3), p. 15 (2009).